Relating megathrust seismogenic behavior and subduction parameters via Machine Learning at global scale

Lucas Crisosto[1] and Andrés Tassara[1]

[1]Universidad de Concepción

July 15, 2024

Abstract

We investigate the relationship between the seismogenic behavior of global megathrusts and various subduction parameters. We performed a parametric approach by implementing three decision tree-based Machine Learning (ML) algorithms to predict the b-value of the frequency-magnitude relationship of seismicity as a non-linear combination of subduction variables (subducting plate age and roughness, slab dip, convergence speed and azimuth, distance to closest ridge and plate boundary). Using the Shapley Additive exPlanations (SHAP) to interpret the ML results, we observe that plate age and subduction dip are the most influential variables. The results suggest that older, shallow-dipping plates contribute to low b-values, indicating higher megathrust stress. This pattern is attributed to the higher rigidity of older plates, increasing flexural strength, and generating a shallow penetration angle, increasing the frictional interplate area and intensifying the megathrust stress. These findings offer new insights into the non-linear complexity of seismic behaviour at global scale.

Relating megathrust seismogenic behavior and subduction parameters via Machine Learning at global scale

Lucas Crisosto[1] and Andrés Tassara[2]

[1]Departamento de Geofísica, Facultad de Ciencias Físicas y Matemáticas, Universidad de Concepción, Concepción, Chile.

[2]Departamento de Ciencias de la Tierra, Facultad de Ciencias Químicas, Universidad de Concepción, Concepción, Chile.

Corresponding author: Lucas Crisosto (acrisosto@udec.cl)

Key Points:

- Non-linear relationship between subduction parameters and seismogenic behaviour represented by b-value are exhibited.
- Plate age and subduction angle are shown as the most impactful parameters in megathrust stress worldwide.
- Older subducting plates with lower subduction angles are associated with lower b-values, implying higher megathrust stress, and viceversa.

Abstract

We investigate the relationship between the seismogenic behavior of global megathrusts and various subduction parameters. We performed a parametric approach by implementing three decision tree-based Machine Learning (ML) algorithms to predict the b-value of the frequency-magnitude relationship of seismicity as a non-linear combination of subduction variables (subducting plate age and roughness, slab dip, convergence speed and azimuth, distance to closest ridge and plate boundary). Using the Shapley Additive exPlanations (SHAP) to interpret the ML results, we observe that plate age and subduction dip are the most influential variables. The results suggest that older, shallow-dipping plates contribute to low b-values, indicating higher megathrust stress. This pattern is attributed to the higher rigidity of older plates, increasing flexural strength, and generating a shallow penetration angle, increasing the frictional interplate area and intensifying the megathrust stress. These findings offer new insights into the non-linear complexity of seismic behaviour at global scale.

Plain Language Summary

We carried out a study to investigate how certain characteristics of subduction zones, where one tectonic plate slides under another, influence the earthquakes behaviour. Using different machine learning algorithms we examined how different variables in these zones affect the relative amount of small versus large earthquakes, parameterized by the slope of a log-normal relationship between frequency and magnitude of events, known as the b–value. Our analysis showed that the age of the subducting plate and the angle at which it dips under another plate are the most influential factors in earthquake behaviour. In particular, we found that older plates with shallow subduction angles are associated with higher stress at the subduction interface, which in turn, increases the probability of large earthquakes, decreasing the b-value. This is because older, colder plates are more rigid than young and hot plates, which increases their resistance to bending, augmenting the contact area between the plates and the friction between them. These findings shed light on the complex dynamics of seismic activity on a global scale and provide valuable information for understanding the earthquake behaviour worldwide.

1. Introduction

The largest earthquakes on Earth occur at convergent plate boundaries along the seismogenic zone of subduction megathrust. The physical properties of subduction zones vary according to the region and affect the stress state that, in turn, influences their seismogenic behavior (Nishikawa & Ide, 2014). To characterise the stress state, different proxies have been used in the literature, such as the maximum recorded magnitude, the seismicity rate or the slope of the log-normal frequency-magnitude distribution of seismicity, known as the b-value of the Gutenberg-Richter law (Gutenberg & Richter, 1944). Regarding this latter, laboratory experiments and natural examples suggest that the stress state and the b-value have a negative correlation, with larger stresses associated with lower b-values because of a dominance of large earthquakes over small events (Scholz, 1968; Wiemer & Wyss, 1997; Schorlemmer et al., 2005; Spada et al., 2013; El-Isa and Keaton, 2013; Scholz, 2015; Petruccelli et al., 2019). A correlation between type of faulting, dominant focal mechanism and the b-value in California, Japan and elsewhere, allows Schoerlemmer et al. (2005) to propose that this parameter can be used as a “stress-meter” that depends inversely on differential stress, a conclusion supported by Scholz (2015) who provided an empirical linear expression for this inverse correlation using data for a wide range of tectonic settings around the globe. Several authors have reported global variations in this parameter at subduction zones, reflecting changes in the stress state along the megathrust (e.g., Carter & Berg, 1981; Nanjo et al., 2012; Kagan & Jackson, 2013; Nishikawa & Ide, 2014). By the other hand, a number of studies have attempted to clarify the factors that influence the stress state and thus the seismogenic behaviour and seismic potential of the megathrust (e.g Heuret et al., 2011; Heuret et al., 2012; Schellart & Rawlinson, 2013; Brizzi et al, 2018; van Rijsingen et al., 2018; Lallemand et al., 2018). Pioneering studies (Ruff & Kanamori, 1980; Kanamori, 1983) have suggested that the largest earthquakes seem to occur at subduction zones where the subducting plate is young and the rate of subduction is high. However, this assumption would be inconsistent with the seismicity documented during the 21st century (i.e. Stein and Okal, 2007). On the other hand, Nishikawa & Ide (2014) and Scholz (2015) have found remarkable correlations between stress levels measured by the b-value and both plate age and slab pull force. These results allow them to suggest that a younger subducting plate would be associated with a higher buoyancy, which generates a higher normal stress on the upper plate and therefore a lower b-value.

Previous works have been mainly based on the recognition and quantification of possible correlations via linear regression between different parameters characterising the kinematics and dynamics of subduction zones by one hand and their seismogenic behaviour by the other (e.g. Ruff & Kanamori, 1980; Heuret et al., 2011; Schellart & Rawlinson, 2013; Nishikawa & Ide, 2014). However, the actual relationship between these parameters is likely non-linear which justifies the implementation of Machine Learning (ML) methods that are recommended to understand the nonlinear interdependence between factors influencing processes like seismic behaviour in various areas (e.g Jones et al., 2020; Xiong et al. 2021). Among these methods, the work of Schafer & Wenzel (2019) stands out, where an attempt is made to cluster zones of maximum magnitude based on input of subduction parameters and similarity between areas according to different properties.

In this study, measurements of subduction parameters and b-values were conducted across 157 transects (Figure 1a), covering most of subduction zones worldwide. The aim was to assess how these variables collectively affect megathrust stress, represented by the b-value. For this, three supervised regression ML algorithms were employed to analyze relationships among input variables and predict the b-value. Subsequently, an interpretation of the generated ML models was carried out using the Shapley Additive exPlanations (SHAP) values (Lundberg & Lee, 2017), which allowed us to understand the contribution of each feature in the prediction of the b-value, enhancing our understanding of processes that regulate the stress state in the megathrust.

2. Data and Methods

We created an ensemble of 157 trench-perpendicular transects (Figure 1a), covering most of the subduction zones for which a 3D model of slab geometry is available in the Slab2.0 model (Hayes et al., 2018). We selected one transect every ~2 degrees along the trench axis of these subduction zones segments. For each, we quantified a number of subduction parameters and computed one b-value as described below grouped in Dataset S1.

2.1 Quantification of geometric and kinematic parameters of subduction zones

For each studied transect we computed values of all the parameters listed in Table S1, as explained in the caption of Figure S1. Convergence velocity (vc_10 in Table S1), azimuth angle (ang_conv in Table S1) and oceanic plate age at the trench (age in Table S1) were derived from the plate kinematics model of Müller et al. (2016), interpolating their grids at the intersection of each transect with the trench. Seafloor roughness was derived from the General Bathymetric Chart of the Oceans (GEBCO) bathymetry. To quantify the roughness, the standard deviation of the bathymetry with respect to a polynomial fit along a transect perpendicular to the trench was calculated oceanward (roughness in Table S1, based in Lallemand et al., 2018). To measure the distance along the trench between each transect and both the oceanic plate edge and the nearest ridge (Dse and Dcr in Table S1), ArcGIS Pro software was implemented directly with its basemap as a reference. Finally, the subduction angle between 0 and 60 km depth (ang_60 in Table S1) was obtained from the Slab2.0 model of Hayes et al. (2018). The distribution of all the subduction parameters is shown in Figure S19 in Supporting Information S1.

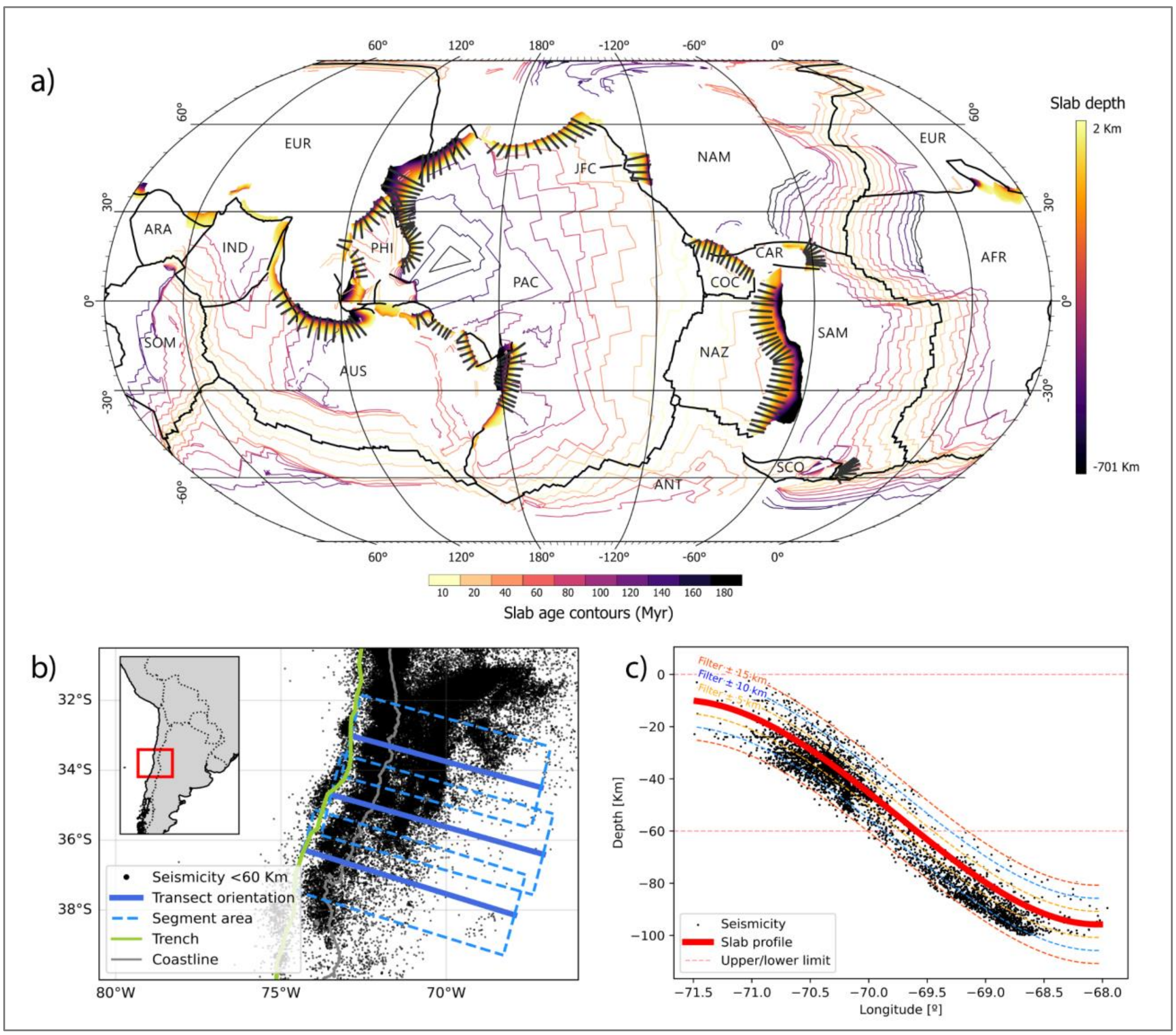

Figure 1. Distribution of transects perpendicular to the trench for the quantification of subduction parameters and b-value. In Figure 1a, the overall distribution of transects in major subduction zones is depicted (dark lines), showing the depth to the subducting plate as reported by the Slab2.0 model (Hayes et al., 2018), in addition with seafloor age contours provided by the grid of Müller et al. (2016). Figure 1b provides a close-up view of the areas from each transect along central Chile, emphasising the 25% overlap with neighbouring segments. The estimation of the b-value for each transect considers seismicity located 200 km at bouth sides of the transect. Figure 1c illustrates an exemplary depth profile of seismicity for one of the transects. Different filters at distances of ±5, ±10, and ±15 km relative to the slab upper surface are applied to evaluate the sensitivity of the b-value estimation to this choice. Figure 1a tectonic plates abbreviations: EUR = Eurasian, ARA = Arabian, IND = Indian, NAM = Northamerican, CAR = Caribbean, JFC = Juan de Fuca, PAC = Pacific, PHI = Philippine, SOM = Somalian, AUS = Australian, NAZ = Nazca, SAM = Southamerican, COC = Cocos plate, SCO = Scotia, ANT = Antartic, AFR = African.

2.2 Estimation of *b*-value

We use the seismicity catalogue provided by the International Seismological Center (ISC) between years 1900 and 2022. To estimate the b-value for each studied transect, we consider earthquakes with epicentres within an area extending 200 km laterally on both sides of the transect (Figure 1b). We consider a 25% overlap between each transect to capture the spatial variability of seismic activity (Figure 1b). Four sub-catalogues were then created for each transect considering either all the recorded events or earthquakes located around the slab upper surface at depths between ±5, ±10 and ±15 km of the Slab2.0 model (Hayes et al., 2018, see Figure 1c). From these sub-catalogues, magnitude differences between correlative events were calculated and the b-value was estimated using the b-positive method proposed by van der Elst (2021). This method, which follows the same form as the maximum likelihood estimator (Aki, 1965), only considers positive magnitude differences to avoid incompleteness problems and the sequences of aftershocks associated with the seismic catalogue. After exploring the sensitivity of resulting b-values to the selected distance threshold to the slab upper surface, we decided to show results considering events within ±10 km of the slab (see Supporting Information S1, Figures S2-S4, for tests with other filters).

2.3 Machine Learning

Figure S22 represents the methodological flow carried out throughout this study. We applied three ML algorithms based on decision trees: CatBoost, GradientBoosting and XGBoost (details in Text S1 in Supporting Information S1), selected for their ability to handle complex data and provide robust performance with small datasets (Friedman, 2001; 2018; Zou et al., 2022). Focused on regression problems, these algorithms aim to predict a target variable (b-value in our case) from a set of input features (subduction parameters). The use of three different supervised ML algorithms is driven by our quest for convergence in conclusions, ensuring consistency in results and strengthening the reliability of interpretations.

For the model's construction, the data were randomly split into training (90%) and test (10%) sets. Subsequently, a cross-validation was performed on the training set to build and validate models using subsets of the data (more details in Text S1 in Supporting Information S1). Here an optimal set of hyperparameters is determined for each algorithm defining the models. Once optimised the hyperparameters for each algorithm and built a model with optimal performance, we evaluated its performance on unseen test data, using metrics such as the Coefficient of Determination (R2), Root Mean Square Error (RMSE) and Mean Absolute Error (MAE) (see details in Text S1 in Supporting Information S1).

To interpret the inner functioning of the model, SHAP value method (Lundberg and Lee, 2017) is implemented. This approach examines the effect of each feature on the predicted outcomes by controlling for the presence of features, which allows us to better understand the decision-making process of the model (Text S2 in Supporting Information S1). In other words, the SHAP value allows us to quantify the influence of each feature (subduction parameter) on the predicted outcome (b-value).

Finally, to analyse the stability of the feature importance in the interpretation of the models, additional tests were performed with different data partitions (80/20 and 70/30) (Figures S7 and S8 in Supporting Information S1). This approach, applied to a small dataset of 157 observations, allows to evaluate the robustness of the constructed models and their sensitivity to specific data partitions. Specific details on metrics and performance of each algorithm are in Supporting Information S1 (Table S2 and Figures S5-S6, S9-S12).

3. Results

The map in Figure 2 shows the global distribution of the estimated b-values only using earthquakes for ±10 km around the slab upper surface. We computed similar maps considering earthquakes ±5 and ±15 km around the slab surface and all available earthquakes (Figure S2 in Supporting Information S1). As can be concluded by comparing Figure 2 with Figure S2, the obtained b-values are not very sensitive to this election, something that is also apparent in Figure S4 where we show for each transect the mean b-value averaging the different slab filters with standard deviation commonly lower than 0.15 (i.e. a 20-25% of the observed range of variations of computed b-values in Figure 2).

A significant variation in the b-values is observed in different regions of the world. For the South American zone, a high variability is observed, with values close to 0.8 dominating and areas of increased b-value coinciding with the subduction of the Juan Fernandez and Carnegie ridges. Likewise, in Cascadia, Sumatra and Aleutians, low b-values (<0.75) predominate, indicating high stress of the megathrust. b-values close to 1 representing moderate stress are found in the Marianas, Philippines and Tonga-Kermadec. For the Sandwich, Caribbean, Philippines and Central America zones, trends towards b-values higher than 1 are observed. The highest b-value (near 1.4), indicating lowest stress, is observed particularly for the Central American zone.

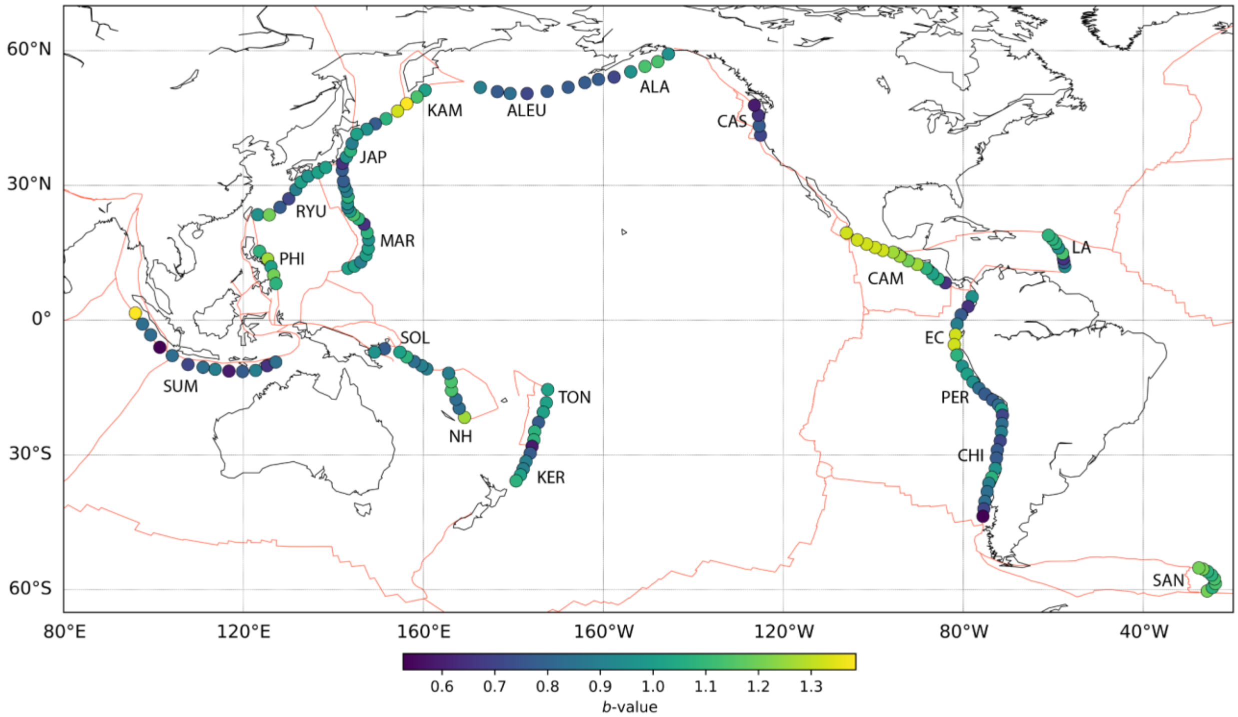

Figure 2. Computed b-values for each transect considering seismicity recorded within ± 10km of the slab upper surface.

The performance of the three ML algorithms is analysed below based on the metrics provided by R^2 as a measure of the percentage of variability explained by the independent variables in the target variable (other metrics are presented in Table S2 of Supporting Information S1). We focus on results obtained with a 90/10 ratio between training and test data (results with lower ratios are also shown in the Supporting Information S1, Figures S7-S12)

Overall, at a ratio of 90/10, all three algorithms were found to have considerable predictive ability, with R2 values of 0.83, 0.88 and 0.82 for XGBoost, GradientBoosting and CatBoost, respectively (Figure S5 in Supporting Information S1) and predicted residual errors lower than 0.15-0.2 (Figure S6). When interpreting the ML models using SHAP values, regardless of the algorithm and the proportion of training and test data used, a consistency in the data patterns can be seen, despite an expected degradation in the performance quality (lower R^2 and larger residuals) for lower training/test ratios (compare Figures S7 and S8 with Figure 3, and S9-S12 with S5-S6). In Figure 3, we present the detailed interpretation of the models with SHAP values for a 90/10 partition of the data, revealing how the input variables contribute to the prediction of the output variable. Similar SHAP values for 80/20 and 70/30 partitions can be found in Figures S7 and S8, and tests for b-values computed considering seismicity within ±5 and ±15 km from the slab upper surface along with their statistical indicators are shown in Figures S8 to S13.

From the bar plots in Figures 3a, c, and e, we observe that the subduction variables having the largest impact in predicting the b-value for the three ML algorithms are consistently the plate age, the subduction angle (ang_60), and the distance to the closest slab edge (Dse). In both GradientBoosting and XGBoost (Figure 3c and e), the plate age and subduction angle are ranked in first and second place, respectively, while in CatBoost (Figure 3a), this order is inverted.

Notably, when examining the summary plot for the three models (Figures 3b, d and f), we can discern a clear trend in the impact of plate age and subduction angle. For instance, we can see that older subducting plates (red dots) are associated with negative SHAP values that predict low b-values, and vice versa. Conversely, the impact of the subduction angle is observed in the opposite way, where smaller dip angles (blue dots) have negative contributions in the SHAP values and therefore in low b-values, and vice versa. The trend for the impact of the distance to the closest slab edge (Dse) is less clear than the other two variables, showing some variability and outliers in its impact on predictions (no clear trend from red to blue or viceversa along the x-axis).

The remaining variables (ang_conv, vc_10, Dcr, and roughness) reveal distinct patterns and less relevant contributions to the predictive models. Convergence azimuth angle (ang_conv), while displaying a generally low impact, exhibits a noteworthy trend where smaller to medium angles (i.e. orthogonal to semi-oblique convergence) consistently contribute to low b-values. In the case of convergence velocity (vc_10), all three algorithms present an unclear trend. High values contribute both positively and negatively, rendering its impact ambiguous.

For Dcr, a consistent observation emerges, particularly pronounced in CatBoost and Gradient Boosting: predominantly low Dcr (i.e. when the transect is closer to a subducting ridge) contribute positively to predictions and therefore are associated with high b-values, while large Dcr have a negative impact predicting low b-values. Finally, the subducting plate roughness is consistently indicated as the variable with the least impact across all three algorithms. In addition, its relationship with b-value via SHAP value remains unclear, adding an element of complexity to its role in shaping the predictive accuracy of the models.

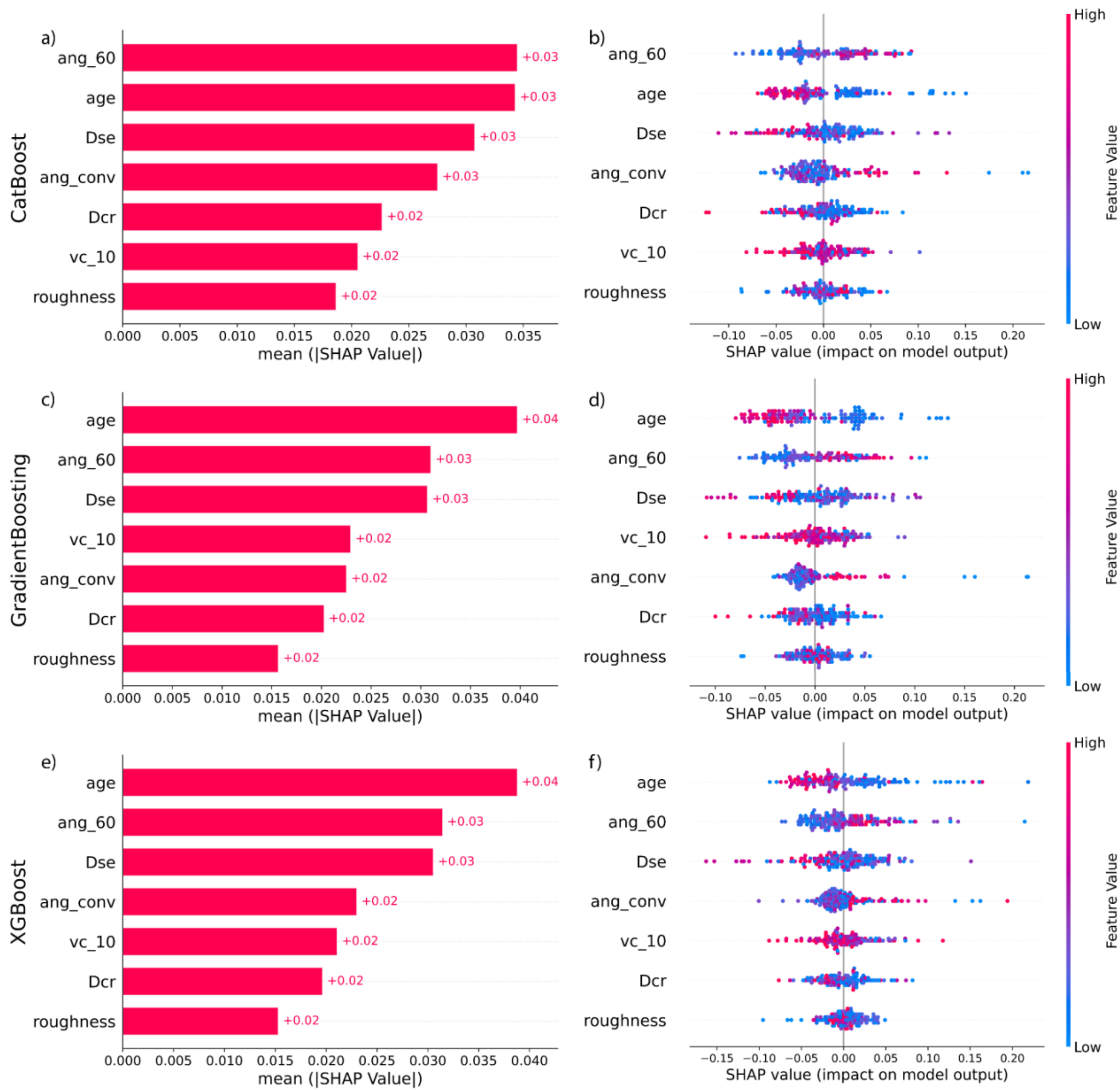

Figure 3. Comparison of feature importance in predicting the b-value for three different models, each trained with a 90/10 train-test partition and using each of the three ML algorithms. Figures 3a, c, and e show the mean absolute SHAP values for each variable for each model, indicating the impact of variables ordered by highest to lowest relevance. Figures 3b, d, and f show the relative contribution of each feature to the predictions of the ML model. The points on the horizontal axis represent the magnitude of the impact of each feature, where positive SHAP values contribute to higher predictions and negative SHAP values contribute to a lower prediction in the model. The color of each point indicates the value of the feature for that sample, with blue for low values and red for high values. The vertical line in the center reflects the mean value of the model's predictions. ang_60 = subduction angle between 0 – 60 km depth; ang_conv = convergence azimuth; vc_10 = convergence velocity: Dse = distance between each transect and the closest slab edge along the trench; Dcr = distance between each transect and the closest subducting ridge along the trench, roughness = seafloor roughness 250 km seaward from the trench.

The differences observed between the models can be attributed to various technical factors inherent in each algorithm. Although both GradientBoosting and XGBoost use boosting methods to build sequential decision trees, they show differences in their inner workings, with

GradientBoosting (Bentéjac et al., 2021). Despite this, both show consistent results in this study, with GradientBoosting showing even better metrics in some cases. However, both algorithms are effective in regression problems, working with continuous variables and allowing effective modelling of non-linear relationships. On the other hand, CatBoost is optimised to handle categorical variables (Prokhorenkova et al., 2018), which could affect the way continuous variables are handled and prioritised. This could consequently affect the interpretation of the results and the consistency in the importance of the variables between the different algorithms, as observed in the prediction of the estimated b-value with seismicity at 5 and 15 km around the slab (Figures S13 and S14 in Supporting Information S1).

4. Discussions and conclusions

Results obtained in this study reveal that oceanic plate age at the trench is the subduction parameter with a greater influence on the b-value and therefore on the stress state of the megathrust. In a first glance, this conclusion seems to agree with Nishikawa & Ide (2014, herein N&I14), who found that plate age has the highest correlation coefficient (0.60) in a linear regression against *b*-value, with convergence velocity and upper plate velocity away from the trench having a rather weak or null correlation. However, the positive correlation between slab age and b-value observed by N&I14, which for them implies a dominance of the age-dependent slab buoyancy on megathrust stress state, is at odds with our results since younger subducting plates (blue dots in Figures 3b, d and f) are associated to positive SHAP values translating into greater b-values, and vice versa.

Although we believe that using a linear univariate correlation approach to analyse the likely complex non-linear interaction of different variables is less efficient than using ML, we still computed a linear correlation between our estimates of b-value (as seen in Figure 2) and subducting plate age at the trench, just to repeat the analysis of N&I14 and to have a better base for comparison (see Figure S20b in Supporting Information S1). We found a very weak and negative correlation, with a coefficient of -0.12. We tested this correlation using b-values computed with all the seismicity around each transect (Figure S20d) and only events inside ±5 and ±15 km from the slab upper surface (Figures S20a and S20c), reinforcing this very weak and negative correlation. We made the same analysis using only events between 1978 and 2009, as done by N&I14 (Figure S21), finding a somehow stronger negative correlation (coefficients between -0.18 and -0.23).

This notable disagreement, which challenges the main conclusions of N&I14, can be due to several factors. First, our linear correlation (Figure S20) was computed considering almost two times more data points than N&I14 (157 versus 75), covering subduction areas that were excluded from their analyses (Alaska-Aleutians, Cascadia, Southern Chile, Lesser Antilles, Sandwich). We also note that for some regions included in both analyses (e.g. Sumatra, Central America) we obtain very different estimates of b-value compared with N&I14. These differences likely own to differences in: the seismicity catalogue used by both studies (ANSS by N&I14 v/s ISC by us), the time interval considered (1978-2009 by N&I14 v/s 1900-2022 by us), the hypocentral depths of considered events (all events by N&I14 v/s only those around the slab upper surface by us), and the method to compute the b-value (maximum likelihood without declustering of aftershock sequences by N&I14 v/s b-positive by us). Particularly this latter point can be significant, since considering only the positive magnitude differences between consecutive events to perform the b-positive method (van der Elst, 2021), instead of all absolute magnitudes as the classical maximum likelihood method (Aki, 1965), means that aftershock sequences are naturally avoided. This ensures that aftershocks, which are known to not obey the Gutenberg-Richter law, cannot contaminate the overall estimate of the b-value, something particularly relevant in areas that experienced great earthquakes during the considered time interval (like in Sumatra-Java between 2004 and 2007, South-Central Chile between 2010 and 2015, or Alaska 2020-2021).

Accepting that our b-value estimates are well-computed, and they can be considered a good representation of the stress state at subduction megathrusts, then we must discuss an alternative conceptual model to the one proposed by Nishikawa and Ide (2014). For this we also consider the large impact that our ML models unravel for the subduction angle as a predictor of the b-value (high average SHAP values in Figures 3a, c and e). Moreover, our results indicate a positive correlation between both parameters, with shallower/smaller subduction angles (blue dots in Figures 3b, d and f) associated with negative SHAP values meaning lower b-values. The combined trend of b-value being negatively correlated to plate age and positively correlated with the subduction angle indirectly implies a reverse correlation between these two subduction parameters, something that is partially supported by recent linear regression analysis at global scale (i.e. Hu and Gurnis, 2020), although a role of plate motion in controlling slab dip seems to be dominant (Cruciani et al., 2005; Lallemand et al., 2005). Into this framework, we propose a novel conceptual model (Figure 4) where the oceanic plate age exerts its dominance via a control on flexural rigidity of the slab, more specifically on the elastic thickness of the plate. In our model, the elastic core of older and colder plates is thicker than for younger and hot plates, and therefore they tend to subduct with larger radius of curvature generating shallow subduction angles (Wu et al., 2008; Capitanio and Morra, 2012). This setting further implies a larger contact area between both converging plates across the megathrust and a wider seismogenic zone because of colder conditions, augmenting thus the the potential for larger earthquakes to occur. Therefore, zones with older subducting plates will tend to have a greater proportion of large earthquakes, impacting in a smaller b-value.

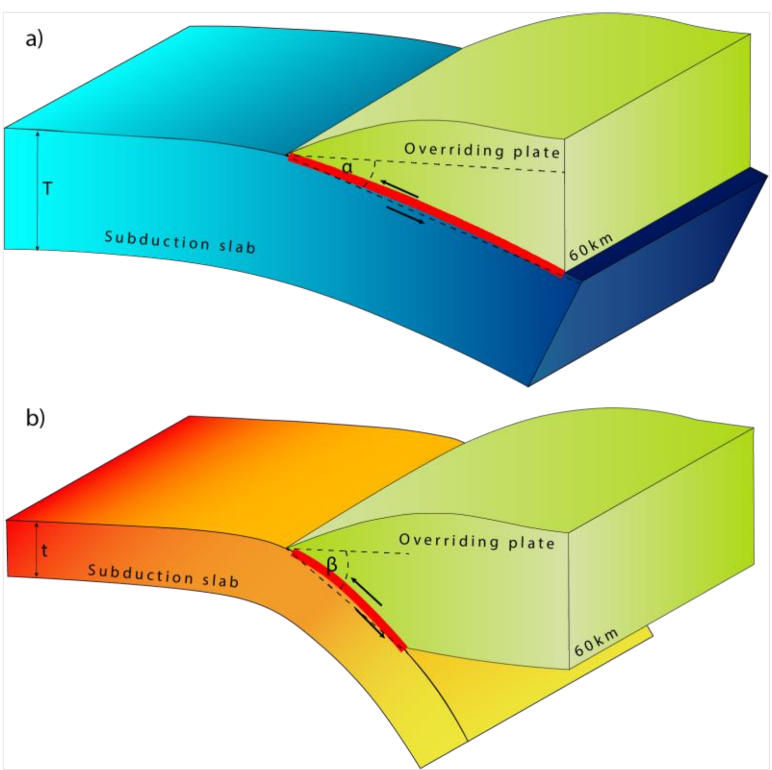

Figure 4. Conceptual model comparing subduction zones characterised by old (a) and young (b) oceanic plates. An older, thicker (T), and more rigid plate subducts at a shallower angle (σ), which increases the contact surface (red line) and the overall stress on the megathrust. A younger, thinner (t), more flexible plate subducts at a steeper angle (β), which reduces the interplate contact surface (red) and the stress on the megathrust.

Our results also suggest that other parameters might play a secondary role modulating the stress state of the megathrust. The distance to the lateral boundaries of subducting plates (Dse in Figure 3) seems to be only marginally less significant than the subduction angle, with transects faraway from boundaries having the lowest b-values and therefore highest stresses. This is in agreement with previous researchers (i.e. Schellart and Rawlison, 2013) that found a relative large linear univariate correlation of Dse with the maximum magnitude of megathrust earthquakes. Plate convergence appears to have a secondary impact compared to previously discussed parameters, somewhat in line with global linear regressions (Nishikawa and Ide, 2014; Hu and Gurnis, 2020). However, it stands in Figures 3b, d and f that most rapid and orthogonal convergence favours low b-values and large megathrust stresses, as can intuitively be supposed. This is in agreement with the findings of Heuret et al. (2011), who found that fast subduction zones with cold plates are associated with large plate interfaces, resulting in higher seismic rates. Although the calculated b-values seems to be much less sensitive to the proximity to a subducting aseismic ridge and the roughness of the oceanic crust, our results suggest that megathrust strength tend to be lower (i.e. higher b-values) in subduction areas dominated by ridge subduction. This can be also appreciated in Figure 2 for South America for example, where subduction of the Carnegie Ridge near 5ºS and Juan Fernandez Ridge at 33ºS are clearly related to locally augmented b-values compared to adjacent regions. This has been observed by previous studies in the region (Legrand et al., 2012) and supports the notion that subducting rough bathymetry associated to seamount chains decrease the strength of the megathrust and favour convergence absorption via creep and aseismic slip (i.e. Wang and Bilek, 2014; Basset and Watts, 2015), contributing to low seismic coupling (Lallemand et al., 2018; van Rijsingen et al., 2018, 2019) and reducing the probability of a large magnitude earthquakes.

The complexity of the likely non-linear interactions between subduction variables in terms of their integrated effect over the megathrust stress state means that using ML approaches, as done here, to analyse the possible influence of each variable in the context of all other existing variables is superior compared to previous uni- or multi-variate linear regressions. This underscores the need for a more holistic approach when interpreting seismic phenomena, highlighting the importance of the interrelation of multiple factors in predicting the seismic behaviour of the megathrust. Future works in this line should include other parameters that have been also indicated as significantly affecting the seismogenic behavior, as the thickness of subducting sediment (e.g. Brizzi et al., 2021), gravity anomalies (e.g. Basset and Watts, 2015; Molina et al., 2021) or temperature (Hyndman, 2023). These considerations emphasize the need for future research to explore more factors, enhancing our understanding of the complex interactions between subduction variables and megathrust stress.

Acknowledgments

We thank Millenium Nucleus CYCLO-NCN19_167 and Fondecyt 1240862 for their financial support.

Open Research

For obtaining earthquakes events for each subduction zone, we used the ISC bulletin catalog (http://www.isc.ac.uk/iscbulletin/search/catalogue/). Convergence velocity and convergence angle were obtained from Müller et al. (2016) cinematic model implemented in GPlates (Müller et al. 2018) software. Plate age was also obtained from Müller et al. (2016) but implemented in ArcGISPro. The global bathymetric grid to calculate seafloor roughness and to measure the distance to the closest ridge was downloaded from GEBCO Gridded Bathymetry Data (https://www.gebco.net/data_and_products/gridded_bathymetry_data/#global). The subduction angle was calculated from Slab2.0 model (Hayes et al. 2018) implemented in ArcGISPro software (Esri, 2020) version 2.6. From the same model and software, we measured the distance to the closest subducting slab edge. Maps were created both with python libraries matplotlib (Caswell et al., 2020), geopandas (Jordahl et al., 2019) and ArcGISPro (Esri, 2020) version 2.6.

References

Aki, K. (1965). Maximum likelihood estimate of b in the formula log N= a-bM and its confidence limits. *Bull. Earthquake Res. Inst., Tokyo Univ.*, *43*, 237-239.

Basset, D., & Watts, A. B. (2015). Gravity anomalies, crustal structure, and seismicity at the subduction zones: 2. Interrrelationships between fore-arc structure and seismogenic behavior. Geochemestry. *Geophysics*, *16*(5).

Barazangi, M., & Isacks, B. L. (1976). Spatial distribution of earthquakes and subduction of the Nazca plate beneath South America. *Geology*, *4*(11), 686-692.

Bentéjac, C., Csörgő, A., & Martínez-Muñoz, G. (2021). A comparative analysis of gradient boosting algorithms. Artificial Intelligence Review, 54, 1937-1967.

Brizzi, S., van Zelst, I., Funiciello, F., Corbi, F., & van Dinther, Y. (2020). How sediment thickness influences subduction dynamics and seismicity. *Journal of Geophysical Research: Solid Earth*, *125*(8), e2019JB018964.

Capitanio, F. A., & Morra, G. (2012). The bending mechanics in a dynamic subduction system: Constraints from numerical modelling and global compilation analysis. *Tectonophysics*, *522*, 224-234.

Carter, J. A., & Berg, E. (1981). Relative stress variations as determined by b-values from earthquakes in Circum-Pacific subduction zones. Tectonophysics, 76(3-4), 257-271.

Caswell, T. A., Droettboom, M., Lee, A., Hunter, J., Firing, E., Sales De Andrade, E., ... & Ivanov, P. (2021). matplotlib/matplotlib: REL: v3. 3.1. Zenodo.

Chen, T., & Guestrin, C. (2016). Xgboost: A scalable tree boosting system. In *Proceedings of the 22nd acm sigkdd international conference on knowledge discovery and data mining* (pp. 785-794).

Chiba, K. (2020). Stress state along the western Nankai Trough subduction zone inferred from b-values, long-term slow-slip events, and low-frequency earthquakes. *Earth, Planets and Space, 72(1)*, 3.

Cruciani, C., Carminati, E., & Doglioni, C. (2005). Slab dip vs. lithosphere age: no direct function. *Earth and Planetary Science Letters*, *238*(3-4), 298-310.

Esri. (2020). ArcGIS Pro (Version 2.7) [Software]. Redlands, CA: Environmental Systems Research Institute, Inc. https://www.esri.com/en-us/arcgis/products/arcgis-pro/overview

Friedman, J. H. (2001). Greedy function approximation: a gradient boosting machine. *Annals of statistics*, 1189-1232.

GEBCO Bathymetric Compilation Group 2020 (2020). The GEBCO_2020 Grid - a continuous terrain model of the global oceans and land. British Oceanographic Data Centre, National Oceanography Centre, NERC, UK. doi:10.5285/a29c5465-b138-234d-e053-6c86abc040b9

Gutenberg, B., & Richter, C. F. (1944). Frequency of earthquakes in California. Bulletin of the Seismological society of America, 34(4), 185-188.

Hayes, G. P., Moore, G. L., Portner, D. E., Hearne, M., Flamme, H., Furtney, M., & Smoczyk, G. M. (2018). Slab2, a comprehensive subduction zone geometry model. *Science*, *362*(6410), 58-61.

Heuret, A., Lallemand, S., Funiciello, F., Piromallo, C., & Faccenna, C. (2011). Physical characteristics of subduction interface type seismogenic zones revisited. Geochemistry, Geophysics, Geosystems, 12(1).

Heuret, A., Conrad, C. P., Funiciello, F., Lallemand, S., & Sandri, L. (2012). Relation between subduction megathrust earthquakes, trench sediment thickness and upper plate strain. *Geophysical Research Letters*, *39*(5).

Hyndman, R. D. (2023). The thermal regime of NW Canada and Alaska, and tectonic and seismicity consequences. Geochemistry, Geophysics, Geosystems, 24(7), e2022GC010570.

Hyndman, R. D., Yamano, M., & Oleskevich, D. A. (1997). The seismogenic zone of subduction thrust faults. *Island Arc*, *6*(3), 244-260.

Hu, J., & Gurnis, M. (2020). Subduction duration and slab dip. Geochemistry, Geophysics, Geosystems, 21(4), e2019GC008862.

International Seismological Centre (2024), On-line Bulletin, https://doi.org/10.31905/D808B830

Jarrard, R. D. (1986). Relations among subduction parameters. *Reviews of Geophysics*, *24*(2), 217-284.

Jones, G. P., Hickey, J. M., Di Stefano, P. G., Dhanjal, C., Stoddart, L. C., & Vasileiou, V. (2020). Metrics and methods for a systematic comparison of fairness-aware machine learning algorithms. *arXiv preprint arXiv:2010.03986*.

Jordahl, K., Van den Bossche, J., Wasserman, J., McBride, J., Gerard, J., Fleischmann, M. & Greenhall, A. (2019). geopandas/geopandas: v0. 6.0. *Zenodo*.

Jordán, T. E., Isacks, B. L., Allmendinger, R. W., Brewer, J. A., Ramos, V. A., & Ando, C. J. (1983). Andean tectonics related to geometry of subducted Nazca plate. *Geological Society of America Bulletin*, *94*(3), 341-361.

Kagan, Y. Y., & Jackson, D. D. (2013). Tohoku earthquake: A surprise? *Bulletin of the Seismological Society of America*, *103*(2B), 1181-1194.

Kanamori, H. (1983). Magnitude scale and quantification of earthquakes. *Tectonophysics*, *93*(3-4), 185-199.

Lallemand, S., Heuret, A., & Boutelier, D. (2005). On the relationships between slab dip, back-arc stress, upper plate absolute motion, and crustal nature in subduction zones. *Geochemistry, Geophysics, Geosystems*, *6*(9).

Lallemand, S., Peyret, M., van Rijsingen, E., Arcay, D., & Heuret, A. (2018). Roughness characteristics of oceanic seafloor prior to subduction in relation to the seismogenic potential of subduction zones. Geochemistry, Geophysics, Geosystems, 19(7), 2121-2146.

Legrand, D., Tassara, A., & Morales, D. (2012). Megathrust asperities and clusters of slab dehydration identified by spatiotemporal characterization of seismicity below the Andean margin. *Geophysical Journal International*, *191*(3), 923-931.

Lemenkova, P. (2020). GEBCO gridded bathymetric datasets for mapping Japan Trench geomorphology by means of GMT scripting toolset. *Geodesy and Cartography*, *46*(3), 98-112.
Lundberg, S. M., & Lee, S. I. (2017). A unified approach to interpreting model predictions. *Advances in neural information processing systems, 30*.

Molina, D., Tassara, A., Abarca, R., Melnick, D., & Madella, A. (2021). Frictional segmentation of the Chilean megathrust from a multivariate analysis of geophysical, geological, and geodetic data. *Journal of Geophysical Research: Solid Earth, 126(6)*, e2020JB020647.

Müller, R. D., Seton, M., Zahirovic, S., Williams, S. E., Matthews, K. J., Wright, N. M., ... & Cannon, J. (2016). Ocean basin evolution and global-scale plate reorganization events since Pangea breakup. *Annual Review of Earth and Planetary Sciences*, *44*, 107-138.

Müller, R. D., Cannon, J., Qin, X., Watson, R. J., Gurnis, M., Williams, S., ... & Zahirovic, S. (2018). GPlates: Building a virtual Earth through deep time. Geochemistry, Geophysics, Geosystems, 19(7), 2243-2261.

Nanjo, K. Z., Hirata, N., Obara, K., & Kasahara, K. (2012). Decade-scale decrease inb value prior to the M9-class 2011 Tohoku and 2004 Sumatra quakes. *Geophysical Research Letters*, *39*(20).

Natekin, A., & Knoll, A. (2013). Gradient boosting machines, a tutorial. *Frontiers in neurorobotics*, *7*, 21.

Nishikawa, T., & Ide, S. (2014). Earthquake size distribution in subduction zones linked to slab buoyancy. *Nature Geoscience*, *7*(12), 904-908.

Nishikawa, T., & Ide, S. (2015). Background seismicity rate at subduction zones linked to slab-bending-related hydration. *Geophysical Research Letters, 42(17),* 7081-7089.

Ogata, Y. (1988). Statistical models for earthquake occurrences and residual analysis for point processes. *Journal of the American Statistical association*, 9-27.

Prokhorenkova, L., Gusev, G., Vorobev, A., Dorogush, A. V., & Gulin, A. (2018). CatBoost: unbiased boosting with categorical features. *Advances in neural information processing systems, 31*.

Ruff, L., & Kanamori, H. (1980). Seismicity and the subduction process. *Physics of the Earth and Planetary interiors*, *23*(3), 240-252.

Schäfer, A. M., & Wenzel, F. (2019). Global megathrust earthquake hazard—maximum magnitude assessment using multi-variate machine learning. *Frontiers in Earth Science*, *7*, 443496.

Schellart, W. P., & Rawlinson, N. (2013). Global correlations between maximum magnitudes of subduction zone interface thrust earthquakes and physical parameters of subduction zones. *Physics of the Earth and Planetary Interiors, 225,* 41-67.

Scholz, C. H. (2015). On the stress dependence of the earthquake b value. *Geophysical Research Letters*, *42*(5), 1399-1402.

Scholz, C. H. (1968). The frequency-magnitude relation of microfracturing in rock and its relation to earthquakes. Bulletin of the seismological society of America, 58(1), 399-415.

Schorlemmer, D., Wiemer, S., & Wyss, M. (2005). Variations in earthquake-size distribution across different stress regimes. *Nature*, *437*(7058), 539-542.

Spada, M., Tormann, T., Wiemer, S., & Enescu, B. (2013). Generic dependence of the frequency-size distribution of earthquakes on depth and its relation to the strength profile of the crust. *Geophysical research letters, 40(4),* 709-714.

Stein, S., & Okal, E. A. (2007). Ultralong period seismic study of the December 2004 Indian Ocean earthquake and implications for regional tectonics and the subduction process. *Bulletin of the Seismological Society of America*, *97*(1A), S279-S295.

Tsapanos, T. M. (1990). b-values of two tectonic parts in the circum-Pacific belt. *Pure and Applied Geophysics, 134*, 229-242.

Tovish, A., Schubert, G., & Luyendyk, B. P. (1978). Mantle flow pressure and the angle of subduction: Non-Newtonian corner flows. *Journal of Geophysical Research: Solid Earth*, *83*(B12), 5892-5898.

Turcotte, D. L., and G. Schubert (1982), Geodynamics: Applications of Continuum Physics to Geological Problems, 450 pp., John Wiley, Hoboken, N. J.

van der Elst, N. J. (2021). B-positive: A robust estimator of aftershock magnitude distribution in transiently incomplete catalogs. *Journal of Geophysical Research: Solid Earth, 126*(2), e2020JB021027.

van Rijsingen, E., Lallemand, S., Peyret, M., Arcay, D., Heuret, A., Funiciello, F., & Corbi, F. (2018). How subduction interface roughness influences the occurrence of large interplate earthquakes. *Geochemistry*, *Geophysics*, *Geosystems*, *19(8)*, 2342-2370.

Van Rijsingen, E., Funiciello, F., Corbi, F., & Lallemand, S. (2019). Rough subducting seafloor reduces interseismic coupling and mega-earthquake occurrence: Insights from analogue models. *Geophysical Research Letters, 46(6)*, 3124-3132.

Wang, K., & Bilek, S. L. (2014). Invited review paper: Fault creep caused by subduction of rough seafloor relief. *Tectonophysics*, *610*, 1-24.

Wiemer, S., & Wyss, M. (1997). Mapping the frequency-magnitude distribution in asperities: An improved technique to calculate recurrence times?. *Journal of Geophysical Research: Solid Earth*, *102(B7)*, 15115-15128.

Wu, B., Conrad, C. P., Heuret, A., Lithgow-Bertelloni, C., & Lallemand, S. (2008). Reconciling strong slab pull and weak plate bending: The plate motion constraint on the strength of mantle slabs. *Earth and Planetary Science Letters*, *272*(1-2), 412-421.

Xiong, Q., Xu, M., Li, J., Liu, Y., Zhang, J., Xu, Y., & Dong, W. (2021). Clinical sequelae of COVID-19 survivors in Wuhan, China: a single-centre longitudinal study. *Clinical microbiology and infection*, *27*(1), 89-95.

Zou, M., Jiang, W. G., Qin, Q. H., Liu, Y. C., & Li, M. L. (2022). Optimized XGBoost model with small dataset for predicting relative density of Ti-6Al-4V parts manufactured by selective laser melting. *Materials*, *15(15)*, 5298